Asian Journal of Geological Research

Volume 6, Issue 3, Page 232-249, 2023; Article no.AJOGER.109623

Lanthanide Tetrad Effects in Stream Sediment Rich- Gold of Betare Oya Area (Cameroon Pan-African Fold Belt, Betare Oya Gold District): Implications for REE- Bearing Phase

Ndema Mbongué Jean Lavenir [a,b*], Christopher Mbaringong Agyingi [a], Sigué Cyrille [a,b], Elong Fanwi Christelle Blessing [a], Nga Essomba Tsoungui Philomène Estelle [b,c] and Ndongfong Edson Fuh [b]

[a] Department of Geology, University of Buea, Cameroon.
[b] Laboratory of Petrology and Structural Geology, Department of Earth Sciences, Faculty of Sciences, UYI, Yaoundé, Cameroon.
[c] National Advanced School of Mines and Petroleum Industries, University of Maroua, Kaele, Cameroon.

Authors' contributions

This work was carried out in collaboration among all authors. Authors EFCB, NEF and NMJL designed the study, performed the statistical analysis, wrote the protocol, and wrote the first draft of the manuscript. Authors EFC and NMJL managed the analyses of the study. Authors SC, CMA and NETPE managed the literature searches. All authors read and approved the final manuscript.

Open Peer Review History:
This journal follows the Advanced Open Peer Review policy. Identity of the Reviewers, Editor(s) and additional Reviewers, peer review comments, different versions of the manuscript, comments of the editors, etc are available here: https://www.sdiarticle5.com/review-history/109623

Original Research Article

Received: 20/09/2023
Accepted: 26/11/2023
Published: 04/12/2023

**Corresponding author: E-mail: jndema2012@gmail.com, jndema2012@mail.com;*

ABSTRACT

Stream sediment surveys were carried out in Betare Oya area and samples collected were analyzed by ICP-MS technology. The purpose of this research was to investigate the geochemical behavior of lanthanides in stream sediment and their implication for REE-bearing phase. The sediments exhibit higher content in Fe_2O_3 (3.96–21.30%), Au (133 - >10000 ppb), Hg (4000 - >10000 ppb), Mn (868-2950), Pb (20.96 - 2950 ppm). The covariance between rare earth element (REE) and Mn suggests that all the REE are incompatible, this implies that the REE are significantly fractionated during differentiation. High rare earth element (510.7-3340.2 ppm) and Y contents were recorded from Betare Oya, the Upper Continental Crust normalized REE patterns show light rare earth element enrichment (La_N/Sm_N: 0.81 – 1.32) relative to heavy rare earth element (Gd_N/Yb_N: 2.26 – 15.32), with a negative Eu anomaly (Eu/Eu*: 0.15 – 0.29). The patterns exhibit tetrad effects showing W- and M- types; the plots of the sizes of tetrad effects with some geochemical parameters allow to characterize two distinct groups of population: the first group involved the majority of samples and the second group encompasses few samples indicating the samples were less affected by terrigenous source materials. The two groups are related to tetrad effect; they can serve as geochemical indicator to determine the environmental conditions. The samples of group 2 have significant tetrad effects (1.88 – 2.28) and sediments indicate non-CHARAC behavior. The enrichment of light rare earth element (LREE) compared to heavy rare earth element (HREE) is due to the presence of monazite. The slight discontinuity in rare earth element (REE) patterns at Nd is the characteristic aspect of tetrad effect for monazite fractionation. The result of this research serves as new evidence for REE dynamics in Cameroon, the contents of REE can be used as background values for further investigations.

Keywords: Stream sediment; Betare Oya; Pan-African fold belt; lanthanides; tetrad effects; non-CHARAC; monazite.

1. INTRODUCTION

The lanthanide Serie include 17 elements from lanthanum to lutetium. This is a coherent group of rare earth elements (REEs) as a result of their position in the periodic table. REEs are distributed in the same way like other trace elements in silicate systems; the sizes of REE cations decrease with increasing atomic number from lanthanum (La) to lutetium (Lu), this is known as the lanthanide contraction and corresponds to progressive filling of an inner electron shell. REEs are mainly divided into light rare earth elements (LREEs) that encompasses lanthanum (La) to europium (Eu) and heavy rare earth elements (HREE) composed of gadolinium (Gd) to lutetium (Lu), and yttrium (Y) [1]. Elements of the lanthanide Serie show similar geochemical properties and provide an understanding of complex processes of a geochemical nature [2].

In geologic environments, the behavior of REEs accounts by differences in their ionic radii and variations in valence states. The tetrad effect phenomenon is a supplementary characteristic for the distribution patterns of lanthanides [3]. Rare earth elements and Y (REE-Y) occur in a trivalent oxidation state (except Ce and Eu), the ionic radii of lanthanides decrease with increasing atomic number from lanthanum to lutetium [4]. When the REEs are normalized with the standards, their charge and radius controlled known as CHARAC process produces smoothed spectra [5]. Also, Y decoupling with respect to holmium (Ho) serves as indicators for the occurrence of non-CHARAC phenomena. The fact that REE patterns have irregular features indicates they are involved in non-CHARAC processes. In order of their atomic number and on the basis of lanthanide complex formation, the REEs are subdivided into four curved components part (La-Nd, Pm-Gd, Gd-Ho, Er-Lu) of their normalized spectrum called tetrad effects [6, 7]. Each rounded line consists of four segments namely first (La-Ce-Pr-Nd), second (Pm-Sm-Eu-Gd), third (Gd-Tb-Dy-Ho) and fourth (Er-Tb-Yb-Lu) tetrads respectively. The middle two elements of each tetrad are fractionated relative to the elements at the edges. This fractionation can be positive or negative, combinations are also possible [8]. The rounded components part are outwards shaped like (convex) or inwards shaped like (concave) and form M- and W- shaped tetrad effect, respectively [6, 8]. M- and W- types tetrad effects point to the opposite behavior of lanthanides at the tetrad boundaries [1, 6]. This means Nd between the first and the second tetrads, Gd between the second and the third. M-type and

W-type tetrad effects are distinct from the quartic f_4^{orth} of a smooth pattern described by λ_4 [9].

In this study, we apply the stream sediment geochemistry to determine the distribution and fractionation of REE, the lanthanide tetrad effect phenomena as well as the implications for REE-bearing phase. The standards of Upper Continental Crust [10] were used to normalize the REE. The size of tetrad effect is calculated after [7]. The second tetrad (Pm - Gd) cannot be determined because praseodymium (Pm) is an artificial element [11]. Also, because of the behavior of Eu^{2+} at low oxygen fugacity and high temperatures in magmatic systems [12].

2. GEOLOGIC SETTING

2.1 Regional Geology

The Betare Oya area (Fig. 1) is found in the Pan-African fold belt in Cameroon [13, 14]. This belt is connected to the Trans-Saharan Belt and extends to NE Brazil [15, 16]. The abundant literature shows that the Pan-African fold belt in Cameroon is composed of:

(1) The Yaoundé domain (YD) is a Neoproterozoic nappe that thrust onto the Congo Craton (Fig. 1). It is made up of Neoproterozoic metasediments and 616 Ma low- to high-grade metasediments [17, 18]. They consist with alkaline magmatism and undergone medium- to high pressure and granulite metamorphism [13].

(2) The present study is carried out in the Adamawa–Yadé domain (AYD; Fig. 1) which is situated between the Sanaga Shear Zone (SSZ) and the Tcholire-Banyo Shear Zone (TBSZ). The AYD is a Paleoproterozoic domain that was affected by the Neoproterozoic orogeny. The AYD is underlined with (a) relicts of Paleoproterozoic rocks; the metamorphism of the granulite facies (2.1 Ga) of this domain was occurred during the Pan-African orogeny, (b) Neoproterozoic (0.7 Ga) materials include low- to medium- grade metasediments and volcanoclastic rocks that were undergone a metamorphism of amphibolite facies and (c) granitoids [19].

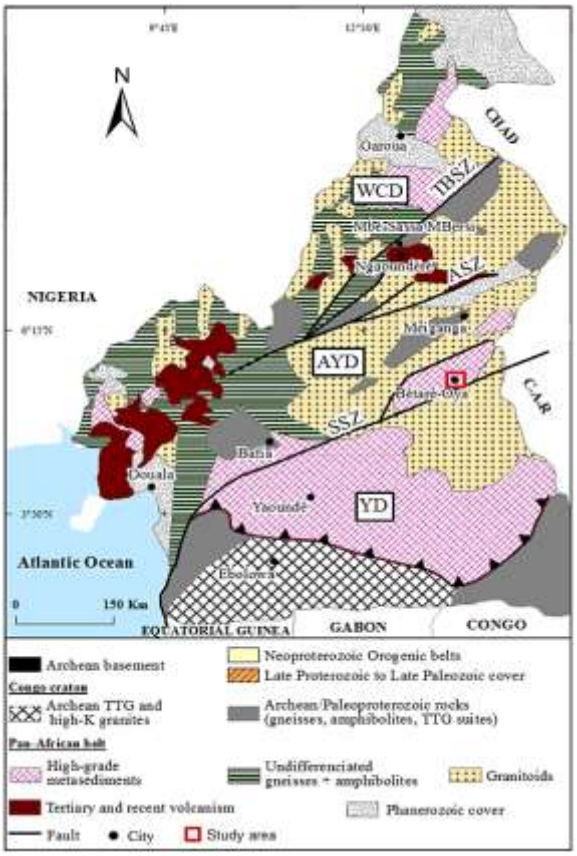

Fig. 1. Geological map of Cameroon showing the study area. ASZ Adamawa Shear Zone, YD: Yaoundé Domain, AYD: Adamawa-Yadé Domain, WCD: Western Cameroon Domain, SSZ: Sanaga Shear Zone, TBSZ: Tchollire-Banyo Shear Zone [14]

(3) The Western Cameroon domain (WCD) occurs along the western edge of the country (Fig. 1) and it is bounded in the southern part by the Adamaoua fault. The WCD is dominated by (a) 830 – 665 Ma (Neoproterozoic) low- to high-grade metasediments and metavolcanites that refer to the Poli Serie; (b) Pan-African (660 – 580 Ma) granitoids including diorites, granodiorites and granites; (c) post-tectonic mafic dykes cross-cut by granites and syenites emplaced at 580 Ma are unconformably with the Poli Serie.

2.2 The geologic of the Betare Oya Area

The Betare Oya area is situated within the Lom Serie which refers to a syn-depositional pull-apart Basin characterized by transtensional movement [20, 21]. The Lom Basin is made up metasedimentary and metavolcanic rocks of Pan-African age. The Betare Oya area is composed of granitoids intrusions (635 ± 5 Ma) associated with gold mineralization. These intrusions are associated to the Central Cameroon shear zones branches, like the Betare Oya shear zones [22]. Other rock units found in the Betare Oya area include metatuff, volcaniclastic rocks, schist, micaschist, quartzite and metaconglomerate horizons. Metasediments are truncated by hydrothermal quartz veins while granitoids include granodiorite and tonalite. The metavolcanic and metasedimentary rocks yield 655 Ma suggesting they were deposited prior to 655 Ma, and metamorphosed between 655 and 585 Ma [23].

3. METHODOLOGY

Twenty active stream sediment samples were collected in the Betare Oya area from a depth of 0.25 – 1.30 m using hand-held digger and the sampling points were plotted in the sample location map (Fig. 2). The samples from the main Lom River and from the first and second-order tributaries were taken randomly above the confluence point. The samples are mainly distributed around the central part of the map, especially along Mari and Bedere Rivers. Chemical analysis was done using inductive coupled plasma mass spectrometry through aqua regia, partial digestion (AR-ICP-MS) at Activation Laboratories (ACTLABS, Canada) to obtain the geochemical concentrations of elements. The sediments were first dry via an oven at 60° and sieving (177 µm) followed by the digestion of 0.5 gram at 90° in a microprocessor-controlled digestion block for two hours. The digested samples are further diluted and analyzed through ICP-MS which represents the most sensitive and flexible method for the analysis of mass fractions of trace elements in geo materials (rocks, mineral, water). Its advantage is in its nearly complete ionization of many elements achieved by the use of argon plasma at temperature of up to 7000°C and fast data acquisition.

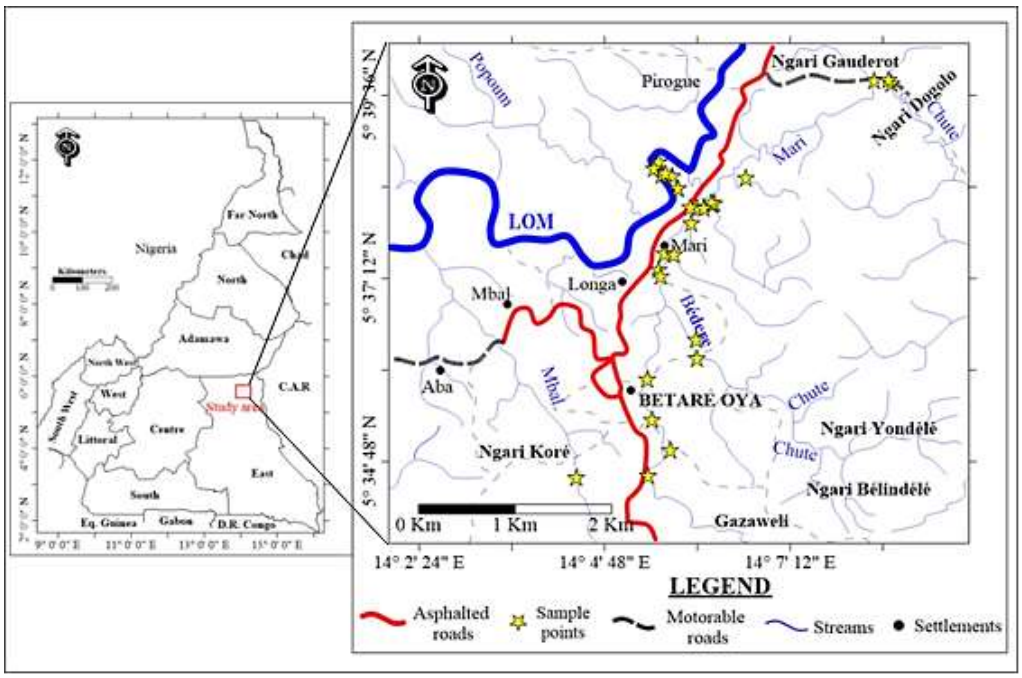

Fig. 2. Sample location map of the study area. Insert: map of Cameroon

4. RESULTS

4.1 Major Elements

The major elements concentrations of stream sediment of Betare Oya are listed in Table 1. Stream sediment exhibits a relative increase in Fe_2O_3 (3.96 – 21.30%; av. = 6.14%), TiO_2 (0.061 – 1.70%), Al_2O_3 (0.19 – 0.60%) compared to the rest of major elements which are closer to their respective detection limit. The graphical inspection shows that the analyzed stream sediment samples are depleted in major elements, they display enrichment only in Fe_2O_3 and TiO_2 (Fig. 3). The increased of Fe_2O_3 and the slight TiO_2 enrichment may be due to the presence of iron oxide and rutile respectively.

4.2 Trace Elements

The concentrations of trace elements are shown in Table 1. The concentration of Hg (4000 to > 10000 ppb), Au (133 to > 10000 ppb), Mn (868 to 2950 ppm; av. = 1836.10 ppm) and Pb (20.96 to 2950 ppm; av. = 200.88 ppm), are very high compared to their respective amount in the Upper Continental Crust (UCC) by [10]. Other elements with high concentrations include Th (50.7 to > 200 ppm), Zn (77 to 255 ppm; av. = 118.31 ppm), Y (24.10 – 163 ppm; av. = 68. 21 ppm) and Cu (8.6 to 222 ppm). Ag (77 to 255 ppm; av. = 118.31 ppm) shows moderate content, while elements like As (< 0.1 to 19.8 ppm), Cd (0.01 to 0.47 ppm) have low values. The large ion lithophile elements (LILEs) including Rb and Ba and high field strength elements (HFSEs) such Ta, Nb, Hf, Zr also display low values respectively (Table 1). The stream sediment samples are depleted in Be, Mo Cd, In, Cs, Hf, Bi, and show enrichment for the rest of trace elements (Fig. 3). High contents of Mn, Th and Zn may be associated with mining activities (gold mining), oxidation and hydrolysis of the primary ore. Higher contents of Hg may be due to the use of Hg in gold separation by the local population in the study area. The high content of Pb indicates the presence of sulfide mineral notably galena.

4.3 Rare Earth Elements

The chemical analyses revealed a wide variation and elevated REE concentrations with ΣREE = 510.7 to 3340.2 ppm (av. = 1992.27 ppm; Table 1). The content of La (108 - > 1000 ppm) and Ce (233 - 2400 ppm, av. = 1051.65 ppm) are higher. Concentrations of Nd (96.7 – 913 ppm) and Gd (12.2 – 128 ppm) is relatively higher, these two lanthanides vary most of all as compared to other lanthanides (III). The order of REEs is Ce > La > Nd > Pr > Sm > Gd > Dy > Tb > Er> Yb > Eu > Ho > Tm > Lu, different to that found in Bwanebwa area [24]. Geochemically, variations of REEs in Betare Oya area can be linked to the loss and gain elements from the parent rocks [25]. The UCC- normalized REE patterns (Fig. 4a) show enrichment in LREE (La_N/Sm_N = 0.81 – 1.32) relative to HREE (Gd_N/Yb_N =2.26 – 15. 32), and a negative Eu anomaly (Eu/Eu* = 0.15 – 0.29). The correlation between REE and Mn (Fig. 4b) suggests that all the REE are incompatible. Therefore, the REE are significantly fractionated during differentiation [26].The concentrations of Fe_2O_3 and Pb are unrelated with REE (Fig. 4c, d).

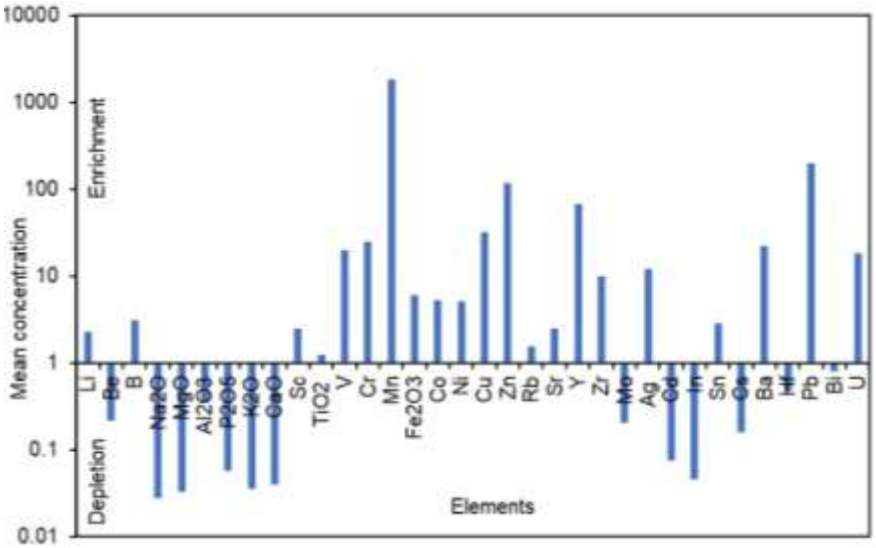

Fig. 3. Enrichment-depletion plot for selected major and trace elements

Table 1. Chemical composition of stream sediment of Betare Oya

Sample	DL	S1	S3	S4	S5	S6	S7	S8	S9	S10	S11	S12	S13	S15	S16	S17	S22	S23	S26	S28	S29
TiO_2 (%)	0.001	1.395	0.976	1.46	1.283	1.591	1.254	1.251	1.069	1.106	1.52	1.231	1.098	0.767	1.001	1.701	1.493	1.191	0.609	1.311	1.289
Na_2O	0.001	0.026	0.024	0.03	0.026	0.027	0.028	0.028	0.026	0.023	0.039	0.026	0.023	0.026	0.027	0.026	0.034	0.023	0.03	0.031	0.028
MgO	0.01	0.05	0.05	0.03	0.03	0.03	0.03	0.07	0.03	0.02	0.03	0.03	0.02	0.02	<0.02	0.03	0.02	<0.02	0.03	0.03	0.05
Al_2O_3	0.01	5.95	4.9	5.76	5.55	6.09	5.8	5.5	4.56	4.75	5.76	5.82	4.46	4.82	5.98	6.55	3.96	4.78	21.3	4.99	5.56
K_2O	0.01	0.04	0.04	0.04	0.02	0.04	0.04	0.05	0.04	0.02	0.04	0.02	0.02	0.04	0.04	0.04	0.04	0.02	0.04	0.04	0.04
P_2O_5	0.01	0.07	0.06	0.04	0.04	0.06	0.04	0.04	0.04	0.04	0.03	0.04	0.03	0.03	0.03	0.04	0.01	0.01	0.06	0.04	0.04
Fe_2O_3	0.01	4.75	6.42	1.97	5.91	6.67	5.55	6.08	1.7	13.45	11.6	11.85	3.25	7.13	5.09	4.87	12.5	8.17	6.72	14.75	4.68
P_2O_5	0.001	0.016	0.073	0.044	0.023	<0.002	0.023	0.048	0.099	0.087	0.06	0.05	0.062	0.066	0.094	0.007	<0.002	0.08	0.128	0.046	0.039
Ag (ppm)	0.002	20.5	4.49	0.074	0.381	0.993	35.9	1.18	3.25	2.65	0.271	40.4	0.693	11	5.93	1.54	26.5	0.202	64.9	0.444	18.9
As	0.1	0.3	< 0.1	< 0.1	< 0.1	< 0.1	< 0.1	< 0.1	< 0.1	< 0.1	< 0.1	< 0.1	< 0.1	< 0.1	< 0.1	< 0.1	< 0.1	< 0.1	19.8	< 0.1	< 0.1
Au (ppb)	0.5	> 10000	> 10000	133	> 10000	> 10000	> 10000	> 10000	> 10000	> 10000	783	> 10000	5580	> 10000	> 10000	> 10000	> 10000	1030	> 10000	1590	8030
B	1	3	2	3	3	3	3	3	3	3	4	3	3	3	3	3	3	3	4	4	3
Ba	0.5	26.7	31.6	26.5	23.6	24.8	25.3	20.1	29.2	11.5	18.2	19.4	15	16.5	15.8	14.4	14.1	36.5	29.8	30	17.5
Be	0.1	0.2	0.2	0.3	0.2	0.2	0.2	0.3	0.3	0.2	0.2	0.2	0.3	0.2	0.2	0.1	0.2	0.3	0.2	0.3	0.1
Bi	0.02	0.48	0.52	0.44	0.43	0.37	0.24	0.56	0.36	0.58	0.65	0.5	0.66	0.45	0.48	0.38	0.83	0.84	6.05	0.5	0.59
Cd	0.01	0.06	0.03	0.05	0.03	0.07	0.01	0.03	0.09	0.02	0.09	0.06	0.07	0.04	0.02	0.02	0.03	0.09	0.47	0.21	0.04
Co	0.1	11.3	5.1	4.9	4.8	5.4	4.5	11.4	3.9	2.6	3.1	3.9	2.6	2.9	3.2	4	3.8	4.3	16.6	3.3	4
Cr	1	18	12	21	22	17	15	21	21	11	17	22	21	23	54	17	32	13	85	41	17
Cs	0.02	0.17	0.31	0.15	0.18	0.2	0.22	0.22	0.18	0.09	0.17	0.14	0.14	0.09	0.12	0.17	0.18	0.08	0.13	0.11	0.17
Cu	0.2	18.6	12.4	14	11.4	25.3	15.8	25	11.1	8.6	17.1	107	13.3	14.1	16.8	12.8	44.6	11.9	222	12.6	24.4
Ga	0.02	0.77	< 0.02	< 0.02	0.36	0.95	0.99	0.04	0.12	< 0.02	< 0.02	< 0.02	< 0.02	< 0.02	< 0.02	1.29	0.66	< 0.02	1.65	1.44	0.18
Ge	0.1	< 0.1	< 0.1	< 0.1	< 0.1	< 0.1	< 0.1	< 0.1	< 0.1	< 0.1	< 0.1	< 0.1	< 0.1	< 0.1	< 0.1	< 0.1	< 0.1	< 0.1	< 0.1	< 0.1	< 0.1
Hf	0.1	1.1	0.3	0.4	0.6	0.7	0.5	0.3	0.4	0.3	0.5	0.3	0.3	0.5	0.4	0.7	0.6	0.4	0.3	0.4	0.4
Hg (ppb)	10	> 10000	> 10000	5190	> 10000	> 10000	7640	5110	5110	8130	5490	> 10000	4360	9860	7450	7670	4000	8360	> 10000	4090	> 10000
In	0.02	0.04	0.04	0.05	0.05	0.03	0.03	0.05	0.05	0.03	0.04	0.04	0.06	0.04	0.06	0.04	0.11	0.04	0.03	0.05	0.03
Li	0.1	2.1	2	2.6	1.8	2.1	2	2.9	3.7	1.6	2.7	1.9	2.1	2.3	1.9	2	1.9	2.2	3.1	2.3	2.6
Mn	1	2740	1630	2250	2170	2950	1900	1850	1530	1630	2090	2010	1550	914	868	2340	1790	1720	1240	1750	1800
Mo	0.01	0.13	0.15	0.15	0.11	0.04	0.13	0.12	0.22	0.12	0.12	0.12	0.12	0.17	0.25	0.06	0.03	0.12	1.82	0.08	0.1
Nb	0.1	0.1	0.2	0.4	0.3	< 0.1	0.2	0.6	0.5	0.5	0.7	0.4	0.3	0.2	0.2	< 0.1	< 0.1	1.2	0.6	0.4	0.3
Ni	0.1	4.6	3.3	3.5	3.5	3.9	4.2	6.1	4.3	2.1	2.7	3.8	2.2	3.6	5.1	3.7	2.6	1.7	34.9	3	3.4
Pb	0.1	24.4	28.7	43	30.2	21.3	20.9	44.4	32.1	137	50.4	84.6	46.9	43.2	100	22.6	71	56	2950	66.9	144
Rb	0.1	1.7	1.7	1.6	1.5	1.7	1.7	2	1.6	1	1.6	1.4	1.2	1.4	1.6	1.5	1.4	0.9	1.8	1.4	2

Re	0.001	0.001	< 0.001	< 0.001	< 0.001	< 0.001	< 0.001	< 0.001	< 0.001	< 0.001	0.001	< 0.001	< 0.001	0.001	0.001	< 0.001	< 0.001	< 0.001	0.001	< 0.001	< 0.001
Sb	0.02	0.13	0.12	0.14	0.08	< 0.02	0.12	0.17	0.21	0.12	0.1	0.1	0.09	0.12	0.17	0.04	< 0.02	0.09	9.7	0.08	0.08
Sc	0.1	2.5	3	2.2	3	2.4	2.8	2.3	2.7	2.4	2.1	2.3	2.8	2.2	3.1	3.1	3.9	1.9	1.5	1.9	1.9
Se	0.1	< 0.1	< 0.1	0.3	< 0.1	0.3	0.2	< 0.1	< 0.1	< 0.1	< 0.1	< 0.1	< 0.1	< 0.1	< 0.1	0.3	0.3	< 0.1	< 0.1	< 0.1	0.1
Sn	0.05	1.52	0.9	1.28	1.61	1.06	1.33	0.99	1.41	0.82	1.15	8.88	0.96	2.33	3.72	1.54	1.71	1.17	22.2	1.07	0.98
Sr	0.5	2.8	3	2.5	2.2	2.5	4	2.5	3.4	2.4	2.1	2	1.7	2.8	2.6	2.4	1.5	1.5	2.9	2.5	2.3
Ta	0.05	< 0.05	< 0.05	< 0.05	< 0.05	< 0.05	< 0.05	0.07	< 0.05	0.06	0.09	< 0.05	0.43	< 0.05	< 0.05	< 0.05	< 0.05	0.11	< 0.05	< 0.05	< 0.05
Te	0.02	0.02	< 0.02	< 0.02	< 0.02	< 0.02	< 0.02	< 0.02	< 0.02	< 0.02	< 0.02	< 0.02	< 0.02	< 0.02	< 0.02	< 0.02	< 0.02	< 0.02	0.25	< 0.02	< 0.02
Th	0.1	93.5	> 200	173	194	50.7	97.3	167	> 200	> 200	> 200	> 200	> 200	> 200	> 200	103	99.2	> 200	> 200	> 200	171
Tl	0.02	0.03	0.1	0.03	0.04	0.03	0.06	0.03	0.03	0.02	0.02	0.03	0.02	0.02	0.03	0.02	< 0.02	0.04	0.07	< 0.02	0.03
U	0.1	8.4	21	14.3	16.1	4.1	8.9	13.6	27.1	23.6	21.7	17.5	18.9	45.5	34.7	8.2	7	22.4	18	18.6	14
V	1	14	13	15	18	11	17	16	16	11	13	14	20	16	23	16	20	13	110	15	9
W	0.1	< 0.1	< 0.1	0.1	< 0.1	< 0.1	< 0.1	< 0.1	< 0.1	< 0.1	1	< 0.1	< 0.1	0.2	< 0.1	< 0.1	< 0.1	< 0.1	156	0.4	< 0.1
Y	0.01	42.3	76.8	57.8	66.1	24.2	36.3	46.9	109	78.9	72.1	60.5	63	163	136	31.4	24.1	67.9	77.8	74	54.3
Zn	0.1	151	108	133	89.4	153	89	102	86.8	114	146	126	125	88.9	77	93.8	93.6	147	84.6	103	255
Zr	0.1	31.2	3.2	9.4	17.3	20	14.4	8.5	4.2	3.3	10.1	5.7	6.6	1.1	1.9	18.6	16	8.8	3.9	6.8	10
La	0.5	248	677	434	488	108	236	402	679	747	622	496	535	>1000	911	227	201	662	469	400	325
Ce	0.01	502	1400	889	987	233	493	848	1400	1580	1310	1050	1150	2400	1900	488	437	1410	994	871	691
Pr	0.1	63.3	155	97.7	107	27.9	60.6	94.7	158	176	149	117	126	266	208	59.2	54.1	157	113	99.9	81.4
Nd	0.02	209	538	349	374	96.7	201	336	555	610	510	407	438	913	746	192	179	547	401	357	290
Sm	0.1	32.9	82.6	60.8	65.2	16.5	35.3	55.3	86.8	95.3	85.5	71.9	72.9	>100	>100	32.1	28.6	75.8	72.8	75.1	52.7
Eu	0.1	2	3.7	2.3	2.8	1.1	1.7	2.3	3.5	3.9	3.2	2.6	2.7	5.5	5.2	1.5	1.6	3.4	2.6	2.2	1.9
Gd	0.1	26.5	67.9	45.4	51.9	12.2	25.5	43.8	75.1	76.6	67.3	55.6	57.8	128	98.9	24.2	21.6	65.5	61	56.9	43.1
Tb	0.1	2.9	6.7	4.7	5.5	1.4	2.8	4.4	8.5	7.7	6.7	5.7	5.8	14	10.9	2.5	2.1	6.5	6.9	6.4	4.7
Dy	0.1	13.3	26.7	18.9	22.8	6.7	12.1	17.4	38.7	31	26.4	22	22.7	60.3	47.3	10.7	8.8	25.8	28.3	26.6	19.3
Ho	0.1	1.6	2.9	2.2	2.6	1	1.4	1.8	4.6	3.2	2.9	2.4	2.5	6.9	5.5	1.2	1	2.7	3.2	3	2.2
Er	0.1	3.9	5.9	4.8	5.4	2.7	2.9	3.9	10.2	6.2	6	4.8	5	14.5	11.6	2.7	2	5.3	6.3	6	4.4
Tm	0.1	0.5	0.5	0.4	0.5	0.4	0.3	0.3	1	0.5	0.6	0.4	0.4	1.4	1.1	0.3	0.2	0.5	0.5	0.6	0.4
Yb	0.1	3.3	3.1	2.7	2.8	2.7	1.8	2	6	2.5	3.1	2.4	2.5	7.8	6.2	1.5	1.3	2.7	2.8	3.3	2.5
Lu	0.1	0.4	0.4	0.4	0.3	0.4	0.2	0.3	0.8	0.3	0.4	0.3	0.3	0.9	0.8	0.2	0.2	0.3	0.3	0.4	0.3
ΣREE		1109.6	2970.4	1912	2115.8	510.7	1074.6	1812	3027.2	3340.2	2793.1	2238.1	2422	n.d	n.d	1043.1	938.5	2964.5	2161.7	1908	1518.9
$(La/Sm)_N$		1.14	1.24	1.08	1.13	0.99	1.01	1.10	1.19	1.19	1.10	1.05	1.11	n.d	nd	1.07	1.07	1.32	0.98	0.81	0.93
$(Gd/Yb)_N$		4.02	10.95	8.41	9.27	2.26	7.08	10.95	6.26	15.32	10.85	11.58	11.56	8.21	7.98	8.07	8.31	12.13	10.89	8.62	8.62
Eu/Eu*		0.29	0.21	0.19	0.21	0.34	0.25	0.20	0.19	0.20	0.18	0.18	0.18	n.d	n.d	0.23	0.28	0.21	0.17	0.15	0.17

DL: detection limit n.d: not determined

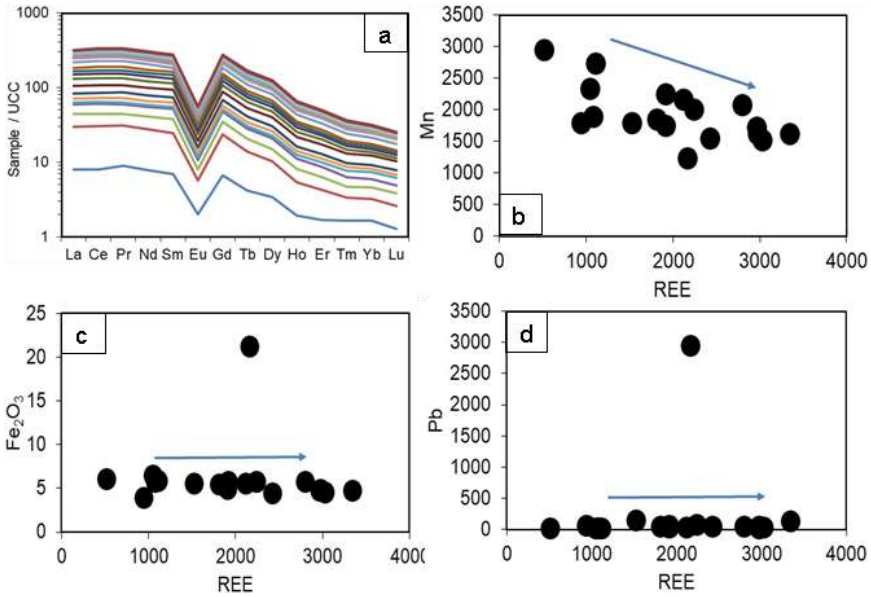

Fig. 4. REE element variation in stream sediment of Betare oya area. (a) UCC- normalized REE patterns of stream sediment samples from Betare Oya, normalization standards from [10]; (b-d) bivariate plots of Fe_2O_3, Mn and Pb relative to REE

5. DISCUSSION

5.1 REE + Y Distribution

REE and yttrium contents for the stream sediment samples of Betare Oya area are presented in Table 1. As aforementioned, the sum of REE is variable and higher (ΣREE = 510.7 to 3340.2 ppm, av. = 1992.27 ppm). The REE-Y abundance in stream sediment samples of Betare Oya area is presented in Table 2. The patterns of REE-Y are similar (Fig. 5a), Ho, Er, Tm, Yb and Lu abundances appear to be lowered constantly from Dy abundances. The concentration of Y, Ho and La/Ho ratio vary from 24 - 163 ppm, 1 to 6.9 ppm and 108 - 245.19 respectively (Table 1, 2). This indicates that Y and Ho have the same behavior in geological environments [27]. For this study, Y accumulation is calculated as Y/Ho ratios and the values vary from 23.62 - 26.48 (Table 2). The plot of Ho vs. Y/Ho ratios is presented in Fig. 5b and it is characterized by two distinct groups of population: the first group (Fig. 5b) displays a wide variation in the scatted plot with Y/Ho ranges from 23.62 – 26.48 (av. = 25) and relatively high Ho (1.8 – 6.9 ppm) values for the majority of samples. The second group yields Y/Ho ratios between 24.10 and 26.44 (av. = 25.37) and low Ho contents. This group encompasses samples S1, S6, S7, S17 and S22. This indicates that samples were less affected by terrigenous source materials leading to decreasing or increasing of Y/Ho ratios. The two groups are linked to common geochemical processes such as tetrad effect and can serve as geochemical indicator to determine the environmental conditions [28]. The concentration of REE-Y is higher, they vary from 1573.2 to 3419.10 ppm in group 1 and 962.6 to 1151.9 ppm in group 2. Mn contents are also higher in the samples: Mn = 868 – 2250 ppm in the first group and 1790 - 2950 ppm in the second group. The covariance among REE-Y and Mn contents (Fig. 5c) suggests that REEs are involved in the formation of minerals that have been derived from pre-existing rocks and transported some distance.

5.2 REEs Tetrad Effect

Mathematically, each tetrad is initially represented by the following function [9].

$$f(x) = \max(0.1 - x^2) = \frac{1 - x^2 + \sqrt{(1 - x^2)^2}}{2}$$

For this study, the size of tetrad, $T_{i\ (i\ =\ 1,\ 3,\ 4)}$ is calculated after [7].

$$T_i = \sqrt{\frac{1}{2} \times \left(\left[\frac{[B_i]}{\sqrt[3]{([A_i^2][D_i])}} - 1 \right]^2 + \left[\frac{[C_i]}{\sqrt[3]{([D_i^2][A_i])}} - 1 \right]^2 \right)}$$

In this relation, [B_i] and [C_i] represent the concentrations of the two central lanthanides in each tetrad, [A_i] and [D_i] refer to the concentrations of the first and the fourth lanthanides of the same tetrad, respectively. The size of each tetrad effect in their respective group was calculated and symbolized with T_1 for the first tetrad (La-Ce-Pr-Nd), T_3 for the third tetrad (Gd-Tb-Dy-Ho) and T_4 for the fourth tetrad (Er-Tm-Yb-Lu). The calculated $T_{i\ (i = 1, 3, 4)}$ values are greater than zero ($T_{i\ (i = 1, 3, 4)} > 0$) indicating tetrad effect [29, 30], and either convex or concave branch [7]. The size, shape of each individual tetrad effect and some geochemical parameters are reported in Table 2. The UCC- normalized REE patterns showing the occurrence of tetrad effect are shown in Fig. 6.

The first (T_1) and third (T_3) tetrad of group 1 yield 0.47 to 0.50 and 0.06 - 0.49 respectively. In the second group T_1 yields 0.27 – 0.45, T_3 ranges from 0.06 to 0.27 and T_4 varies between 0.68 – 7.21. These tetrad effects display convex M- type tetrad effect forms in REE distribution patterns (Fig. 6a, 6b). The size (T_4) of samples S7 (5.22), S17 (4.66) and S22 (7.21) of group 2 is higher (Table 2), this may be due to the fact that this samples are more depleted in HREE compared to the other samples. The fourth tetrad is significant for samples S7, S17 and S22 because the size of tetrad effect is greater than 1.1 [31]. The size of the fourth tetrad (T_4) in group 1 ranges from 0.03 to 0.35 (Table 2), this tetrad illustrates a typical concave W-type shape (Fig. 6a) indicating low-temperature depositional conditions [30]. This tetrad is taken to be significant because its size in the samples is smaller than 0.9 [31].

5.2.1 Correlation between the sizes of tetrad effects T_1, T_3 and T_4

Fig. 7 shows the scatter plots for the size of T_3-T_4, T_4-T_1 and T_3-T_1 in the samples. Two distinct groups of population are identified in the binary graphs with various T_3-T_4, T_4-T_1 and T_3-T_1 values. The first group (Fig. 7a) displays a narrow variation of T_1 (0.47 – 0.50) and T_3 (0.35 – 0.49) while group 2 presents a wide variation in T_1 (0.27 – 0.45) and T_3 (0.06 – 0.27). In Fig. 7b, the first group includes the majority of the samples with a narrow variation in T_3 (0.35 – 0.49) and low in T_4 (0.03 – 0.35) values. The second group involves samples S1, S6, S7, S17 and S22 with a wide variation of T_3 (0.06 – 0.27) and low to high T_4 (0.17 – 7.21) values. Fig. 7c shows a relative wide variation of T_1 (0.27 – 0.45) in group 1 and a low to elevated T_4 (0.17 – 7.21) values. The samples of group 2 cluster at a narrow T_1 and very low T_4 values. As shown in Fig. 7a, T_3 shows positive correlation with T_1, while a linear correlation is observed between T_4 and T_3 in group 2. These plots represent the cartesian coordinate systems [29]; each point has only one x-axis T_3 or T_1 and y-axis T_4 or T_3 respectively.

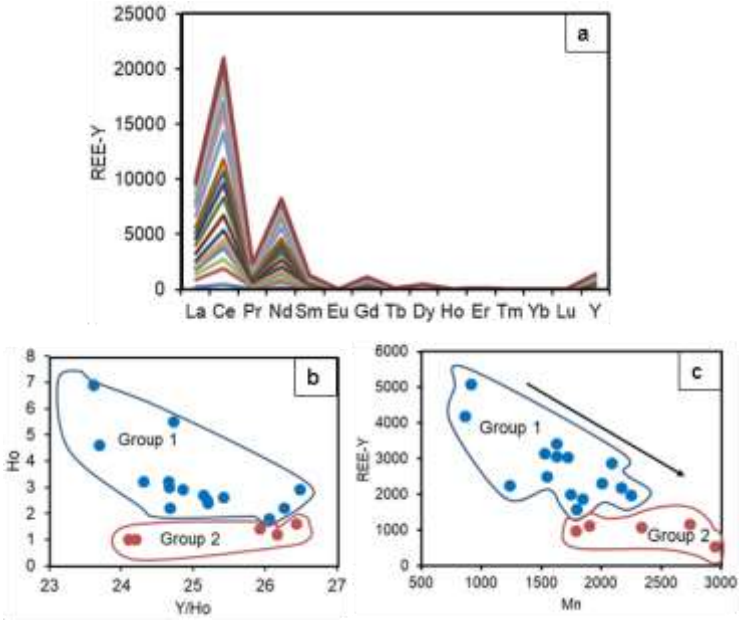

Fig. 5. Chemical composition of stream sediment of Betare Oya. (a) REE-Y abundance patterns, (b) bivariate plot of Y/Ho vs. Ho and (c) REE vs. Mn plot

Table 2. Size, shape of each individual tetrad effect and some geochemical parameters

Tetrad effects		T_1		T_3		T_4		T											
Sample	Group	Shape	Size	Shape	Size	Shape	Size	Size	REE -Y	La/Ho	Zr/Hf	Ho/Y	Y/Ho	Rb/Sr	K/Rb	Y_N/Dy_N	Eu/Eu*	Ce/Ce*	Sr/Eu
S3	1	Concave	0.49	Convex	0.44	Convex	0.04	0.81	3047.20	233.45	10.67	7.25	26.48	0.57	0.02	0.53	0.21	1.02	0.81
S4	1	Concave	0.48	Convex	0.39	Convex	0.03	0.77	1970.10	197.27	23.50	5.50	26.27	0.64	0.02	0.57	0.19	1.02	1.09
S5	1	Concave	0.49	Convex	0.41	Convex	0.21	0.86	2181.90	187.69	28.83	8.67	25.42	0.68	0.01	0.54	0.21	1.02	0.79
S8	1	Concave	0.48	Convex	0.35	Convex	0.20	0.83	1859.10	223.33	28.33	6.00	26.06	0.80	0.02	0.50	0.20	1.02	1.09
S9	1	Concave	0.49	Convex	0.47	Convex	0.28	0.91	3136.20	147.61	10.50	5.75	23.70	0.47	0.02	0.52	0.19	1.01	0.97
S10	1	Concave	0.49	Convex	0.45	Convex	0.08	0.83	3419.10	233.44	11.00	10.67	24.66	0.42	0.02	0.47	0.20	1.03	0.62
S11	1	Concave	0.49	Convex	0.44	Convex	0.03	0.80	2865.20	214.48	20.20	7.25	24.86	0.76	0.02	0.51	0.18	1.01	0.66
S12	1	Concave	0.49	Convex	0.41	Convex	0.18	0.85	2298.60	206.67	19.00	8.00	25.21	0.70	0.01	0.51	0.18	1.03	0.77
S13	1	Concave	0.49	Convex	0.42	Convex	0.18	0.85	2484.60	214.00	22.00	8.33	25.20	0.71	0.02	0.52	0.18	1.04	0.63
S15	1	Concave	n.d	Convex	0.49	Convex	0.35	n.d	n.d	n.d	2.20	7.67	23.62	0.50	0.02	0.50	n.d	n.d	0.51
S16	1	Concave	0.50	Convex	0.48	Convex	0.30	0.92	n.d	165.64	4.75	6.88	24.73	0.62	0.02	0.53	n.d	1.03	0.50
S23	1	Concave	0.49	Convex	0.43	Convex	0.19	0.86	3032.40	245.19	22.00	9.00	25.15	0.60	0.02	0.49	0.21	1.03	0.44
S26	1	Concave	0.49	Convex	0.44	Convex	0.13	0.84	2239.50	146.56	13.00	10.67	24.31	0.62	0.02	0.51	0.17	1.02	1.12
S28	1	Concave	0.48	Convex	0.43	Convex	0.03	0.79	1982.40	133.33	17.00	7.50	24.67	0.56	0.02	0.52	0.15	1.03	1.14
S29	1	Concave	0.47	Convex	0.38	Convex	0.30	0.88	1573.20	147.73	25.00	7.33	24.68	0.87	0.02	0.52	0.17	1.00	1.21
S1	2	Concave	0.45	Convex	0.27	Convex	0.17	0.77	1151.90	155.00	28.36	4.00	26.44	0.61	0.02	0.59	0.29	0.94	1.40
S6	2	Concave	0.27	Convex	0.06	Convex	0.68	0.82	534.90	108.00	28.57	2.50	24.20	0.68	0.02	0.67	0.34	1.00	2.27
S7	2	Concave	0.44	Convex	0.23	Convex	5.22	1.98	1110.90	168.57	28.80	7.00	25.93	0.43	0.02	0.56	0.25	0.97	2.35
S17	2	Concave	0.44	Convex	0.19	Convex	4.66	1.88	1074.50	189.17	26.57	6.00	26.17	0.63	0.02	0.54	0.23	0.99	1.60
S22	2	Concave	0.43	Convex	0.14	Convex	7.21	2.28	962.60	201.00	26.67	5.00	24.10	0.93	0.02	0.51	0.28	0.99	0.94

T: tetrad effects n.d: not determined

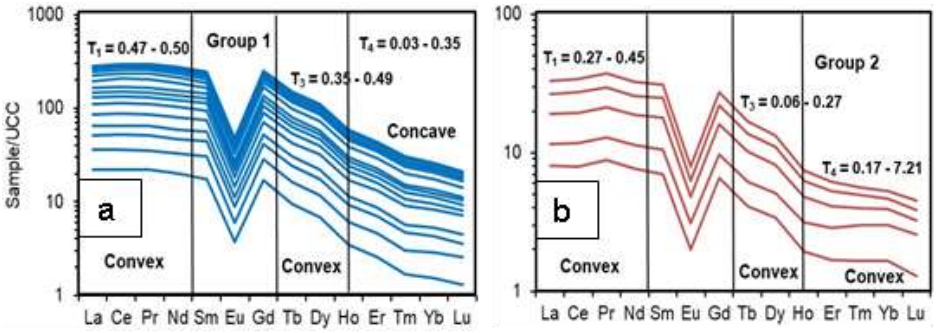

Fig. 6. UCC-normalized REE distribution pattern of the stream sediment samples from Betare Oya showing the tetrad effects and their respective shape

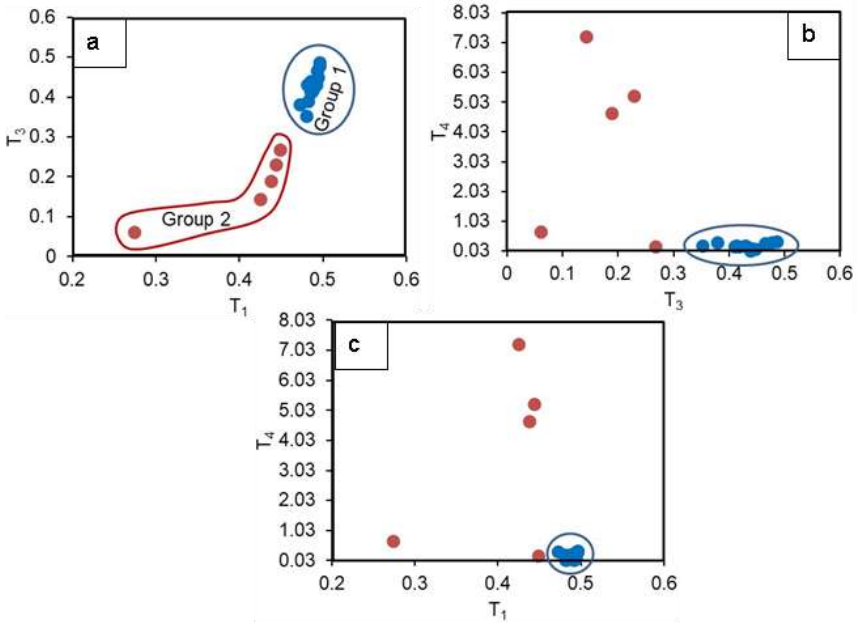

Fig. 7. Scatter plot of the size of T_3-T_1, T_4-T_3, T_4-T_1 tetrad effect for the stream sediment samples of Betare Oya

5.2.1.1 Size of tetrad effect T_1 with some geochemical parameters

The mutual association of T_1 versus some ratios such as La/Ho, Zr/Hf, Y/Ho, Eu/Eu* and Ce/Ce* illustrates two separate groups of T_1 values, suggesting different depositional conditions (Fig. 8a-f). This indicates the non-CHARAC behavior illustrated with the biplot Zr/Hf-Y/Ho (Fig. 8a). In this diagram, the samples of group 1 fall into the field of non-CHARAC with variable Zr/Hf (2.2 - 25) and Y/Ho (23.62 to 26.48) ratio. Samples of group 2 fall in the CHARAC field with Zr/Hf ratio varying from 26.57 to 28.80 and Y/Ho from 24.10 to 26.44.

K/Rb (0.01 – 0.02) ratio displays a narrow variation of T_1 (0.47 – 0.50) in group 1 and a relative high variation in group 2 (K/Rb: 0.2; T_1: 0.27 – 0.45; Fig. 8b). Similar result is obtained with the plot Rb/Sr vs. T_1 in which Rb/Sr = 0.42 – 0.87 in group 1 and Rb/Sr = 0.43 – 0.93 in group 2 (Fig. 8c). Samples of group 2 with K/Rb = 0.2 and Rb/Sr = 0.43 – 0.93 show significant tetrad effects. This indicates the fractionation of Rb and decreasing of K/Rb ratio [12]. In Fig. 8d the first group is characterized by a moderate narrow T_1 values and variable La/Ho ratios (133.33 – 245.15). The second group shows low to moderate T_1 values. T_1 content and La/Ho ratio display a wide range due to the fractionation of LREE [32, 33].

Ho/Y ranges from 2.5 – 10.67 (Fig. 8e); they are low (Ho/Y = 2.5 – 7) in samples S1, S6, S4, S7 and S9 and this is attributed to adsorption of Ho

on Fe and Mn oxides. The (Ho/Y = 6 – 7.67) is constant in samples (S3, S7, S8, S11, S15, S28, S29), and high (Ho/Y = 8 – 10.67) in samples (S5, S10, S12, S13, S23, S26). This is relevant for the predominance of Ho relative to Y. This result is in accordance with the tetrad effect (T_1) values. The higher Ho/Y ratio (Y/Ho = 8 – 10.67) in the samples is due to the presence of ligands in hydrothermal fluids [30, 34]. Two groups of population for the Betare Oya samples are also recorded in the scatter diagram of Zr/Hf ratios vs. T_1 (Fig. 8f). Therefore, we suggest that the stream sediment of Betare Oya area was deposited under two different conditions.

The plot of T_1 against Eu/Eu* (Fig. 9a) also confirms the two distinct groups of population: the samples of group 1 display high T_1 and moderate Eu/Eu* while group 2 shows moderate T_1 and high Eu/Eu*. Eu^{2+} is responsible of negative anomaly in chemical precipitates as seen in Fig. 4a. Furthermore, according to Fig. 9a, the samples of group 1 show a slightly positive trend, whereas the samples of group 2 display a negative trend. Thus, Eu anomalies were probably generated from plagioclase.

The size of T_1 vs. Ce/Ce* is illustrated in Fig. 9b in which Ce/Ce* ratios decrease with the values of T_1 (group 2) and exhibit a very weak positive correlation (group 1). This shows that the sediments of group 1 were precipitated under higher oxygen fugacity conditions. The concave shape tetrad effects in REE patterns and tetrad effect in the computed T_1 (except sample S6 in which T_1 = 0.27) can be related to more stable depositional conditions.

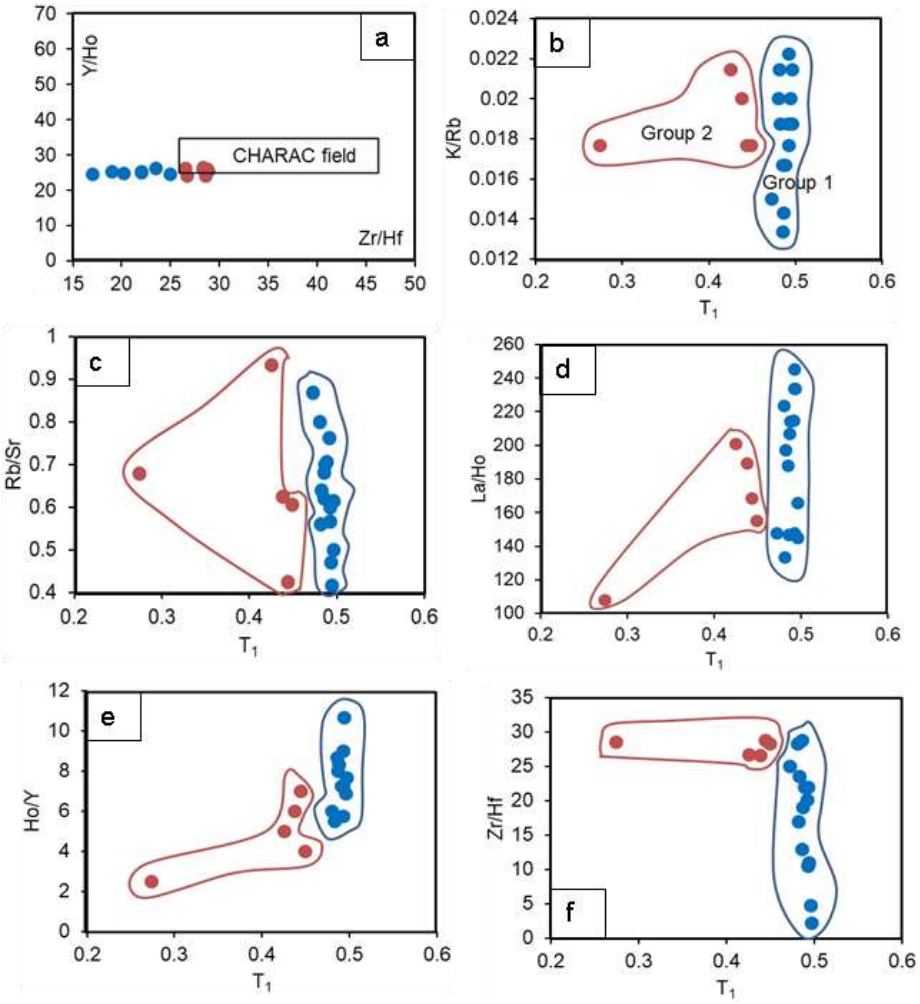

Fig. 8. Bivariate diagrams for the studied stream sediment samples. a) Zr/Hf vs. Y/Ho ratios, the CHARAC field is from [5]. b) K/Rb, c) Rb/Sr, d) La/Ho, e) Ho/Y) and f) Zr/Hf ratios for the calculated T_1

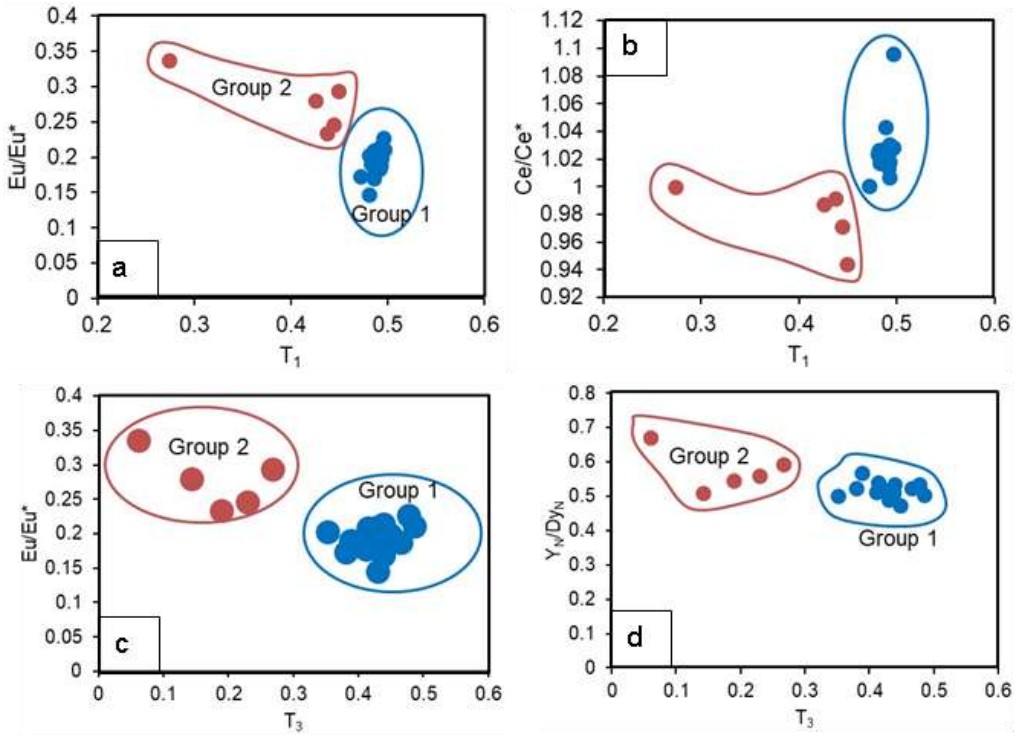

Fig. 9. Bivariate plots of the size of T_1 and T_3 with some geochemical ratios respectively. a, b) plots of Eu/Eu* and Ce/Ce* vs. T_1; c, d) plots of Eu/Eu* and $(Y/Dy)_N$ vs. T_3

5.2.1.2 Association between Eu/Eu, $(Y/Dy)_N$ and the size of T_3*

The relationship between Eu anomaly and tetrad effect are illustrated in the scatter plot Eu/Eu* vs. T_3 (Fig. 9c). The plot shows a negative correlation (group 2) and a slightly positive correlation (group 1) between T_3 and Eu/Eu*. This indicates that the study sediments show an enrichment in LREEs and a negative europium anomaly (Fig. 4a). Therefore, increasing of negative Eu anomalies is related to decreasing tetrad effects [7]. Although anomalies of Eu are explained by feldspar fractionation [35], significant tetrad effects are found at the same time with extremely low Eu concentrations. The $(Y/Dy)_N$ vs. T_3 diagram presents a clear negative correlation between Y and T_3 (Fig. 9d). $(Y/Dy)_N$ contents increase from group 1 (Y_N/Dy_N = 0.47 – 0.53; av. = 0.52) to group 2 (Y_N/Dy_N = 0.51 – 0.67; av. = 0.57). This result is common for the majority of rare earth element deposits.

*5.2.1.3 Relationship between the degree of tetrad effect with Y/Ho, Zr/Hf and Eu/Eu**

To check for the common behavior of tetrad effect, Y/Ho, Zr/Hf and Eu/Eu* are projected against the degree of tetrad effect (T). The total tetrad (T) for N = 3 is determined according to the relation of [7].

$$T = \sqrt{\frac{1}{2N} \times \sum_{i=0}^{N} \times \left(\left[\frac{[B_i]}{\sqrt[3]{([A_i^2][D_i])}} - 1 \right]^2 + \left[\frac{[C_i]}{\sqrt[3]{([D_i^2][A_i])}} - 1 \right]^2 \right)}$$

The degree of the tetrad effect (T) varies from 0.77 to 0.92 in group 1 and 0.77 to 2.28 in group 2 (Table 2). The UCC ratio of Y/Ho ratio is 25.30 [10], and the Y/Ho ratios in this study range from 23.62 to 26.27 (av. = 25) in group 1 and 24.10 to 26.44 in group 2 (av. = 25.37), both similar with the UCC value. The Y/Ho vs. T plot (Fig. 10a) shows a linear correlation and the two group of population display a well define cluster respectively. Three samples of group 2 exhibit Y/Ho ratio that varies from 24.10 – 26.17 display significant tetrad effects with T = 1.88 to 2.28.

In this study, Zr/Hf ratio vary from 2.20 – 28.83 (av. = 17.20) in the first group and 26.57 – 28.80 (av. = 27.79) for the second group (Table 2) implying that sediments are affected by magmatic-hydrothermal alteration [12]. Zr/Hf vs. T binary plot (Fig. 10b) also illustrates a linear trend and the two groups of population display a well define cluster respectively. The samples S7,

S17 and S22 of group 2 with Zr/Hf (26.57 – 28.80) ratio also display significant tetrad effects (T = 1.88 – 2.28 25). The Zr/Hf (av. = 27.79) ratio of the samples of group 2 is almost close to the UCC ratio (Zr/Hf = 36.42), compared to those of group 1 with low Zr/Hf ratio (av. = 17.20).

The stream sediments from the study area show variable Sr/Eu (0.44 – 1.21 in group 1 and 0.94 – 2.27 in group 2) ratios (Table 2). This result is in accordance with the strong negative Eu anomalies (Eu/Eu* = 0.15 – 0.23 in group 1 and 0.23 – 0.34 in group 2). When Eu anomaly is plotted against T (Fig 10c), samples of group 2 with Eu/Eu* = 0.25 – 0.28 have significant tetrad effects (1.88 – 2.28).

5.3 Implications for REE- Bearing Phase

REE- bearing phase includes major (K-feldspar, plagioclase, quartz, biotite) and accessory (apatite, monazite, zircon, xenotime, hingganite) minerals. REE- minerals such as apatite, monazite and garnet are debated to generate REE patterns displaying tetrad effect phenomenon. The studied sediments display high content in REE indicating monazite influence because monazite is the main source of REE. The graphical inspection of the mean concentrations of the studied REEs in comparison to the values of the UCC by [10, 36] is shown in Fig. 11. The plot shows that the REEs from the study area are strongly elevated (REE = 510.7 – 3340.2 ppm, av. = 1992.27 ppm) compared to UCC values (about 15 times the values of UCC). The enrichment of LREE (La_N/Sm_N = 0.81 – 1.32; Table 1) relative to HREE (Gd_N/Yb_N = 2.26 – 15.32) may be due to the presence of monazite which is a monoclinic Ce-phosphate mineral ($CePO_4$) that incorporates large amounts of REE within its structure, meanwhile its crystal structure prefers to accommodate LREE [37]. Contrary, xenotime (YPO_4) is a tetragonal mineral which prefers HREE with smaller ionic radii. These two minerals are insoluble while apatite dissolves rapidly [38]. The slight discontinuity in the group 2 REE patterns at Nd is the characteristic aspect of tetrad effect for monazite fractionation, since modelled REE patterns have revealed the discontinuity at Nd without tetrad effect [39]. The Eu/Eu* of the analyzed sediments yield 0.15 to 0.23 in group 1 and 0.23 – 0.34 in group 2 and calculated T (1.88 – 1.98) values are significant for Eu/Eu* ratio range from 0.23 – 0.28.

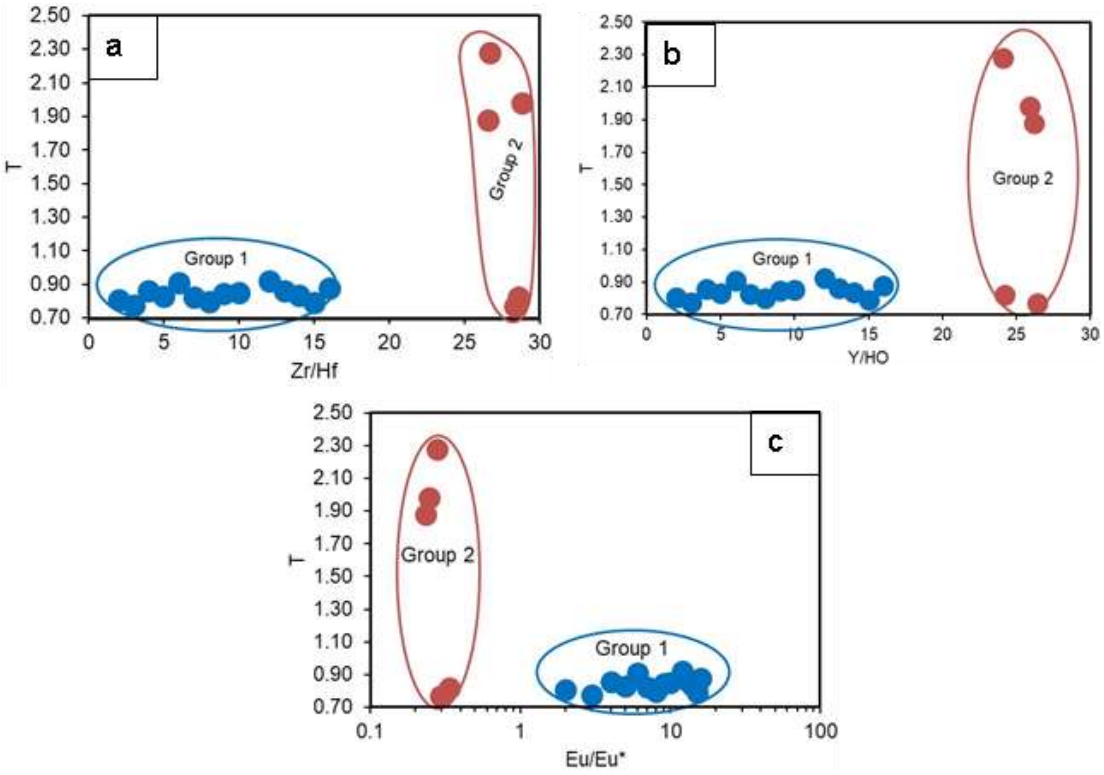

Fig. 10. Plots of Eu/Eu*, Zr/Hf and Y/Ho against the degree of the tetrad effect (T)

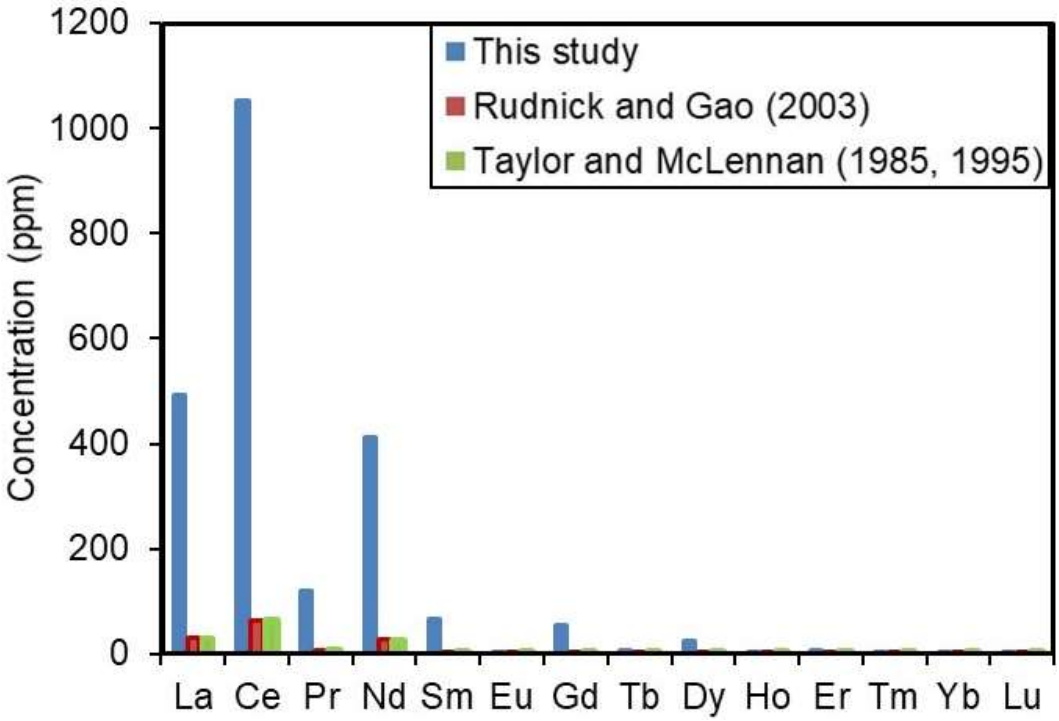

Fig. 11. Graphical representation of the mean concentration of REE in stream sediment of Betare Oya in comparison to the values of the UCC by [10, 36]

6. CONCLUSION

This study provides the first deeper examination of REE in stream sediment of Betare Oya gold district and the results show that:

The stream sediment samples of Betare Oya area exhibit higher content in Fe_2O_3, Au, Hg, Mn and Pb. The sediments show enrichment in Fe_2O_3, TiO_2, Li, B, Sc, V, Cr Mn, Co, Cu, Zn, Rb, Sr, Y, Zr, Ag, Sn, Pb, U, and depletion for the rest of elements. The correlation between REE and Mn suggests that all the REE are incompatible, implying that the REE are significantly fractionated during differentiation. High REE and yttrium concentrations are recorded from the study area, the UCC-normalized REE patterns show LREE enrichment compared to HREE, with a negative europium anomaly. The rare earth element patterns of stream sediment samples of Betare Oya exhibit tetrad effects showing W- and M- types. The plots of the sizes of tetrad effects with some geochemical parameters allow to characterize two distinct groups of population: the first group involved the majority of samples and the second group encompasses some few samples indicating that samples were less affected by terrigenous source materials. All the samples of group 2 with their respective geochemical parameter values have significant tetrad effects (1.88 – 2.28). The two groups are related to tetrad effect and can serve as geochemical indicator to determine environmental conditions and sediments indicate the non-CHARAC behavior. Evident covariance among REE-Y and Mn contents suggests that REEs are involved in the formation of minerals that have been derived from pre-existing rocks and transported some distance. The enrichment of LREE relative to HREE is due to the presence of monazite. The slight discontinuity in REE patterns at Nd is the characteristic aspect of tetrad effect for monazite fractionation.

DISCLAIMER

This paper is an extended version of a preprint document of the same author.

The preprint document is available in this link: https://assets.researchsquare.com/files/rs-2988964/v1/8248bf5b-771d-47ec-8c95-18979f4abe56.pdf?c=1691690856 [As per journal policy, preprint /repository article can be published as a journal article, provided it is not published in any other journal]

ACKNOWLEDGEMENTS

This paper is the result of the fifth author Master thesis research work at the University of Buea. The authors are indebted to anonymous reviewers and editor for their thoughtful and constructive comments.

COMPETING INTERESTS

Authors have declared that no competing interests exist.

REFERENCES

1. Chen Y, Niu Y, Shen F, Gao Y, Wang X. New U-Pb zircon age and petrogenesis of the plagiogranite Troodos ophiolite. Cyprus. Lithos. 2020;362–363:105472. Available:https://doi.org/10.1016/j.lithos.2020.105472.
2. Sukumaran PV. Elements that rule the world: Impending REE metal crisis. J Geol Soc India. 2012;80:295.
3. Peppard DF, Mason GW, Lewey S. A tetrad effect in the liquid–liquid extraction ordering of lanthanides (III). J Inorg Nuclear Chem. 1969;31:2271–2272.
4. Shannon RD. Revised effective ionic radii and systematic studies of interatomic distances in halides and chalcogenides. Acta de Crystallog Bull. 1976;25:925–946.
5. Bau M Controls on the fractionation of isovalent trace elements in magmatic and aqueous systems: Evidence from Y/Ho, Zr/Hf, and lanthanide tetrad effect. Contrib Mineral Petrol. 1996;123:323–333.
6. Masuda A, Kawakami O, Dohmoto Y, Takenaka T. Lanthanide tetrad effects in nature: Two mutually opposite types, W and M. Geochem J. 1987;21:119–124.
7. Monecke T, Kempe U, Monecke J, Sala M, Wolf D. Tetrad effect in rare earth element distribution patterns: A method of quantification with application to rock and mineral samples from granite-related rare metal deposits. Geochim Cosmochim Acta. 2002;66(7):1185–1196.
8. Azizi MR, Abedini A, Alipour S. Application of lanthanides tetrad effect as a geochemical indicator to identify fluorite generations: A case study from the Laal-Kan fluorite deposit NW Iran. Comptes Rendus Géosci. 2020;352:43–58. Available:https://doi.org/10.5802/crgeos.2.
9. Anenburg M, Williams MJ. Quantifying the tetrad effect, shape components, and Ce–Eu–Gd Anomalies in Rare Earth Element Patterns. Math Geosci; 2021. Available:https://doi.org/10.1007/s11004-021-09959-5.
10. Rudnick RL, Gao S. Composition of the continental crust. Treatise on geochemistry. 2003;3:1–64.
11. McLennan SM, Rare earth element geochemistry and the “tetrad” effect. Geochim Cosmochim Acta. (1994);58.
12. Irber W. The lanthanide tetrad effect and its correlation with K/Rb, Eu/Eu*, Sr/Eu, Y/Ho, and Zr/Hf of evolving peraluminous granite suites. Geochim Cosmochim Acta. 1999;63:489–508.
13. Nzenti JP, Njanko T, Tanko Njiosseu EL, Tchoua FM. Les domaines granulitiques de la Chaîne Panafricaine Nord Equatoriale au Cameroun. In: Vicat JP, Bilong JP, editors. Collection GEOCAM I. Géologie et environnement au Cameroun; 1998. French.
14. Toteu SF, Penaye J, Djomani YP Geodynamic evolution of the Pan-African belt in central Africa with special reference to Cameroon. Can J Earth Sci. 2004;41: 73–85.
15. Castaing C, Feybesse JL, Thieblemont D, Triboulet C, Chevremont P. Palaeogeographical reconstructions of the Pan-African/Brasiliano orogen: closure of an oceanic domain or intracontinental convergence between major blocks. Prec Res. 1994;69:327-344.
16. Neves SP, Bruguier O, Vauchez A, Bosch D, Silva JMR, Mariano G. Timing of crust formation, deposition of supracrustal sequences, and Transamazonian and Brasiliano metamorphism in the East Pernambuco belt (Borborema Province, NE Brazil): Implications for western Gondwana assembly. Prec Res. 2006;149: 197-216.
17. Nzenti JP, Barbey P, Macaudiere J, Soba D. Origin and evolution of the late Precambrian high-grade Yaoundé gneisses (Cameroon). Prec Res. 1988;38: 91-109.
18. Ngnotue T, Nzenti JP, Barbey P, Tchoua FM. The Ntui-Betamba high-grade gneisses: a Northward extension of the Pan-African Yaounde gneisses in Cameroon. J Afri Earth Sci. 2000;31:369-381.
19. Toteu SF, Van Schmus WR, Penaye J, Michard A. New U-Pb and Sm-Nd data from north-central Cameroon and its

bearing on the pre-PanAfrican history of Central Africa. Prec Res. 2001;108:45-73.
20. Ngako V, Affaton P, Nnange JM, Njanko JT. Pan-African tectonic evolution in central and southern Cameroon: transpression and transtension during sinistral shear movements. J Afri Earth Sci. 2003;36:207–214.
21. Toteu SF, Penaye J, Deloule E, Van Schmus WR, Tchameni R. Diachronous evolution of volcano-sedimentary basins north of the Congo Craton: insights from U/Pb ion microprobe dating of zircons from the Poli, Lom and Yaoundé Groups (Cameroon). J Afri Earth Sci. 2006;44:428-442.
22. Kankeu B, Greiling RO, Nzenti JP, Bassahak J, Hell JV. Strain partitioning along the Neoproterozoic central Africa shear zone system: Structures and magnetic fabrics (AMS) from the Meiganga area, Cameroon. Neues Jahrbuch für Geologie und Paläontologie Abhandlungen. 2012;265(1):27- 47.
23. Ndonfack K, Xie Y, Zhong R, Yomeun BS, Cui K, Shan X. Tectonic evolution of neoproterozoic rocks, eastern cameroon: implication for gold mineralization in the Betare Oya and Woumbou-Colomine-Kette district. Prec Res; 2021.
Available:https://doi.org/10.1016/j.precamres.2021.106475.
24. Ndema Mbongue JL. Geochemical Fractionation of Lanthanides in Stream Sediments around Bwanebwa Area, Pan-African Fold Belt (Cameroon). I J Trend Scientific Res Develop. 2020;4(3):363-373.
25. Ebyan, OA, Khamis HA, Alia HH, Abed NS. Radioactivity and Geochemistry of Wadi El Reddah Stream Sediments, North Eastern Desert, Egypt. Arab J Nuclear Sci Appl. 2020;53(1):76-87.
26. Davidson J, Turner S, Plank T. Dy/Dy*: Variations Arising from Mantle Sources and Petrogenetic Processes. J Petrol. 2013;54(3):525-537.
27. Gadd MG, Layton-Matthews D, Peter JM. Non-hydrothermal origin of apatite in SEDEX mineralization and host rocks of the Howard's Pass district, Yukon, Canada. Am Mineral. 2016;101:1061–1071.
28. Mackin J. Relationships between Si, Al and Fe deposited on filter covered glass substrates in marine sediments and in suspensions of sediments and standard clays. Marine Chem. 1989;26:101-117.
29. Abedini A, Mansour RA, Calagari AA. Lanthanide tetrad effect in limestone: a tool to environment analysis of the Ruteh Formation, NW Iran. Acta Geodyn Geomat. 2018;15(3)(191):229–246.
30. Mansour RA, Abedini A, Alipour S. Application of lanthanides tetrad effect as a geochemical indicator to identify fluorite generations: A case study from the Laal-Kan fluorite deposit, NW Iran. Comptes Rendus Géosci, Sci Planète. 2020;352(1): 43-58.
31. Yasnygina TA, Rasskazov SV. Rare Earth Element Spectra with Tetrad Effect: Manifestation in Paleozoic Granite of the Oka Zone in the Eastern Sayan Range. Geokhimiya. 2008;8:877–889
32. Shearer CK, Papike JJ, Laul CC. Chemistry of potassium feldspars from three zoned pegmatites, Black Hills, South Dakota: Implications concerning pegmatite evolution. Geochim Cosmochim Acta. 1985;49:663-673.
33. Cosanay P, Kırat E, Çevik N, Kızılkanat C, Mutlu H, Koç S. Geochemical, microthermometric, and isotopic constraints on the origin of fluorite deposits in central Anatolia, Turkey. Turkish J Earth Sci. 2017;26:206–226.
34. Migdisov A, Williams-Jones AE, Brugger J, Caporuscio FA. Hydrothermal transport, deposition, and fractionation of the REE: experimental data and thermodynamic calculations. Chem Geol. 2016;439:13–42.
35. Möller P, Muecke GK. Significance of europium anomaly in silicate melts and crystal-melt equilibria; a re-evaluation. Contrib Mineral Petrol. 1984;87:242-250.
36. Taylor SR, MClennan SM. The Continental Crust; Its composition and evolution; an examination of the geochemical record preserved in sedimentary rocks. Blackwell Oxford. 1985;
37. Ndema Mbongue JL, Sigué C, Nzenti JP, Suh CE. Mineral chemistry (EMPA) of monazites in metamorphic rocks from Edea region: implications of the monazite chemistry on the metamorphic evolution of the Nyong Complex. Arab J Geosci. 2022; 15:1665.
Available:https://doi.org/10.1007/s12517-022-10924-7.
38. Irber W, Förster HJ, Hecht L, Möller P, Morteani G. Experimental, geochemical, mineralogy and O-isotope constraints on the late-magmatic history of the

Fichtelgebirge granites (Germany). Geol Rundsch 86 (suppl.).1997;110-124.

39. Yurimoto H, Duke EF, Papike JJ, Shearer CK. Are discontinuous chondrite-normalized REE patterns in pegmatitic granite systems the results of monazite fractionation? Geochim Cosmochim Acta. 1990;54:2141–2145.

Peer-review history:
The peer review history for this paper can be accessed here:
https://www.sdiarticle5.com/review-history/109623